

Cite this: *Chem. Sci.*, 2017, **8**, 1068

Versatile synthesis and enlargement of functionalized distorted heptagon-containing nanographenes†

Irene R. Márquez,^a Noelia Fuentes,^a Carlos M. Cruz,^a Virginia Puente-Muñoz,^b Lia Sotorrios,^c M. Luisa Marcos,^d Duane Choquesillo-Lazarte,^e Blanca Biel,^f Luis Crovetto,^b Enrique Gómez-Bengoa,^c M. Teresa González,^g Ruben Martín,^h Juan M. Cuerva^a and Araceli G. Campaña^{*a}

Highly distorted polycyclic aromatic hydrocarbons (PAHs) are predicted to be attractive goals in nanoscience owing to the new properties they can exhibit. We have shown that a variety of functionalized distorted heptagon-containing nanographenes can be easily prepared from simple building blocks by a sequence of Co-catalyzed cyclotrimerization and cyclodehydrogenation reactions. The versatility of this strategy allows easy subsequent enlargement of these nanostructures by Ni-catalyzed cross-coupling and final cyclodehydrogenation reactions. Soluble extended distorted nanographenes **1** and **2** containing heptagon and an edge-shared pentagon–heptagon combination have been synthesized. High distortion of the polycyclic backbone of **2** caused by non-hexagonal rings and a helicene moiety was confirmed by X-ray crystallography. Experimental data reveal promising optical and electronic properties for distorted PAHs with long fluorescence lifetimes (up to 14.5 ns) and low band gaps (down to 2.27 eV). This straightforward and versatile synthetic strategy, the observed long fluorescence lifetimes and the small optical and electrochemical band gaps for the presented compounds may promote the future implementation of distorted graphene molecules in electronic devices.

Received 30th June 2016

Accepted 30th August 2016

DOI: 10.1039/c6sc02895k

www.rsc.org/chemicalscience

Introduction

Planar polycyclic aromatic hydrocarbons (PAHs) such as nanographenes and graphene nanoribbons (GNRs) have received significant attention in recent years.¹ PAHs are attractive materials for nanoscale electronic devices due to their tunable non-zero bandgaps, which are principally controlled by their size and edges. Microscopy studies have shown that graphene samples usually include non-hexagonal rings such as pentagons and heptagons, thus leading to curved carbon based nanostructures² which can significantly modify the original properties.³ Particularly, typical topological defects in large area graphene films are disclinations, as individual pentagons or heptagons, and dislocations or grain boundaries, as pairs of pentagons and heptagons, that result in energetically favourable structures.⁴ Unlike commonly studied pentagon-containing PAHs, such as corannulene and its derivatives, which have been extensively synthesized and investigated,⁵ graphene-type molecules containing seven-membered rings are much less common and only very few examples have been reported.

The first synthesis of [7]circulene was reported in 1983 showing a non-planar saddle-shaped geometry.⁶ After these pioneering examples reported by Yamamoto and Nakazaki,

^aDepartamento Química Orgánica, Universidad de Granada (UGR), C. U. Fuentenueva, 18071 Granada, Spain. E-mail: araceligo@ugr.es

^bDepartamento de Fisicoquímica, Facultad de Farmacia, UGR. Cartuja Campus, 18071 Granada, Spain

^cDepartamento de Química Orgánica I, Universidad del País Vasco, E-20018, San Sebastián, Spain

^dDepartamento de Química, Universidad Autónoma de Madrid, c/Francisco Tomás y Valiente no. 7, Cantoblanco, 28049 Madrid, Spain

^eLaboratorio de Estudios Cristalográficos, Instituto Andaluz de Ciencias de la Tierra (CSIC-UGR), 18100 Armilla, Granada, Spain

^fDepartamento de Electrónica y Tecnología de Computadores, Facultad de Ciencias, CITIC, UGR, E-18071 Granada, Spain

^gFundación IMDEA Nanociencia, Ciudad Universitaria de Cantoblanco, E-28049 Madrid, Spain

^hInstitute of Chemical Research of Catalonia (ICIQ), Catalan Institution for Research and Advanced Studies (ICREA), Spain

† Electronic supplementary information (ESI) available: General details, synthesis and spectroscopy data of new compounds and copies of ¹H and ¹³C-NMR spectra of new compounds. Experimental details on optical and electrochemical measurements. Crystal data and structure refinement of compounds **2**, **6a**, **6d** and **6h**. Further details on theoretical calculations and Cartesian coordinates of computed structures. VT-¹H-NMR, 2D-NMR and HRMS spectra of compounds **1** and **2**. CCDC 1485682–1485685. For ESI and crystallographic data in CIF or other electronic format see DOI: 10.1039/c6sc02895k



graphene molecules incorporating heptagons remained forgotten until 2012, when Miao and co-workers reported the synthesis of curved polycyclic aromatic molecules.^{7a} In this case, the introduction of a seven-membered ring in an isoelectronic to planar hexabenzocoronene compound forces the structure out of planarity, increases solubility and enhances fluorescence. Later on, in 2015, they synthesized new saddle-shaped polycyclic arenes containing two heptagons showing a deep distorted structure but with drastically diminished optical properties.^{7b,c} In 2013, Durola and co-workers unexpectedly obtained an unusual hexa[7]circulene due to rearrangement during the Scholl reaction.^{8a} Another structure containing pentagon-heptagon moieties was reported by Kuck in 2012.^{8b}

Scott, Itami and co-workers made a major breakthrough in 2013, synthesizing a grossly warped nanographene with five embedded heptagons around a central pentagon.⁹ The X-ray crystal structure confirmed the distortion caused by the odd-membered rings, drastically enhancing solubility in organic solvents. Comparison with a purely hexagonal nanographene shows that the distortion of the planar sheet affects its electronic and optical properties. The distorted compound exhibits a wider band gap, higher fluorescence and easier oxidation/reduction than the defect-free nanographene. An in depth study of these unconventional heptagon-containing PAHs is still limited owing to the absence of a general, efficient and versatile method for their synthesis. At present, these curved graphene molecules are prepared either from heptagon-containing precursors or by generating the seven-membered rings through cyclodehydrogenation or Friedel-Crafts reactions. Although these approaches have no doubt resulted in interesting and exotic carbon nanostructures, such strategies unfortunately lack flexibility and versatility.

Here, we describe a new and versatile synthetic route to rapidly prepare rather elusive distorted nanographenes containing seven-membered rings *via* intermolecular Co(0)-mediated cyclotrimerization reaction followed by cyclodehydrogenation events from simple acyclic precursors, thus representing a unique tool for rapidly creating molecular diversity (Scheme 1).

Interestingly, we have successfully implemented Ni-catalyzed cross-coupling reactions of aryl methyl ethers *en route* to unprecedented all-carbon distorted nanographenes, thus allowing for counterintuitive strategies for preparing graphene-type motifs.

Results and discussion

Synthetic methodology and structural characterization

We started our investigations by designing a route to **1** (Scheme 1). Although a variety of structurally well-defined expanded nanographenes and graphene nanoribbons (GNRs), exhibiting different widths, lengths, edge structures and heteroatom doping, have been previously synthesized,¹⁰ to the best of our knowledge, compounds **1** and **2** constitute new examples of distorted expanded nanographenes containing a heptagon at the edge of the structure. Moreover, compound **2** has a very unusual polycyclic arene backbone containing adjacent five- and seven-membered carbocycles.^{8b}

To such an end, we studied the key cyclotrimerization using dialkynes **3** (Table 1) that were easily prepared from simple precursors *via* Sonogashira–Hagihara coupling reactions. The presence of the carbonyl group hindered the formation of undesired 9,10-dihydroanthracenes¹¹ while allowing for subsequent functionalization techniques, as recently shown by Miao and co-workers.^{7b} We found that a wide variety of functionalized heptagon-containing polyphenylenes **5a–o** could easily be obtained by using Co(0)-catalyzed intermolecular cyclotrimerization reactions. Noteworthily, the cyclotrimerization reaction tolerates substitution in both coupling partners. Substitution in the benzophenone moiety in dialkynes **3** affords compounds such as **5b**. Dialkynes **3** can also incorporate *meta*- or *para*-substituted ethynylbenzenes affording the corresponding functionalized products **5c–f**. *Meta*- and *para*-substituted diphenylacetylenes **4** are also allowed as in compounds **5g–j**. Furthermore, compounds **5k–n** are relevant examples of cyclotrimerization with substitution in both building blocks simultaneously. The versatility of the strategy is also illustrated in compound **5o** incorporating two thiophene moieties as aromatic rings. With a reliable technique *en route* to seven-membered carbocycles in hand, we envisioned that the distorted-PAHs could be prepared by oxidative cyclodehydrogenation, thus accessing heptagon-containing nanographenes (Fig. 1). The presence of methoxy groups allowed controlling of the regioselectivity in the oxidative aromatic coupling when using 2,3-dichloro-5,6-dicyano-*p*-benzoquinone (DDQ) as an oxidant in acidic media (MeSO₃H).¹²

Intriguingly, we observed partial demethylation and oxidation during the cyclodehydrogenation of **5g**, yielding exclusively **6d**.¹³ Remarkably, incomplete cyclodehydrogenation led to doubly distorted compounds such as **6a** and **6d**, incorporating both the heptagon and [5]-helicene motifs at different positions of the aromatic backbone. Both compounds, **6a** and **6d**, were characterized by X-ray crystallography (Fig. 1b), confirming their highly distorted structure. Hence, these compounds constitute a new family of structures within the helical nanographene arena.^{7a,14} In contrast to the presence of methoxy groups, less activated *tert*-butylated compounds resulted in

Previous work:

- Heptagon-containing starting materials
- Late-stage introduction of heptagons:
 - Intramolecular Friedel-Crafts acylation
 - Intramolecular cyclodehydrogenation

This work:

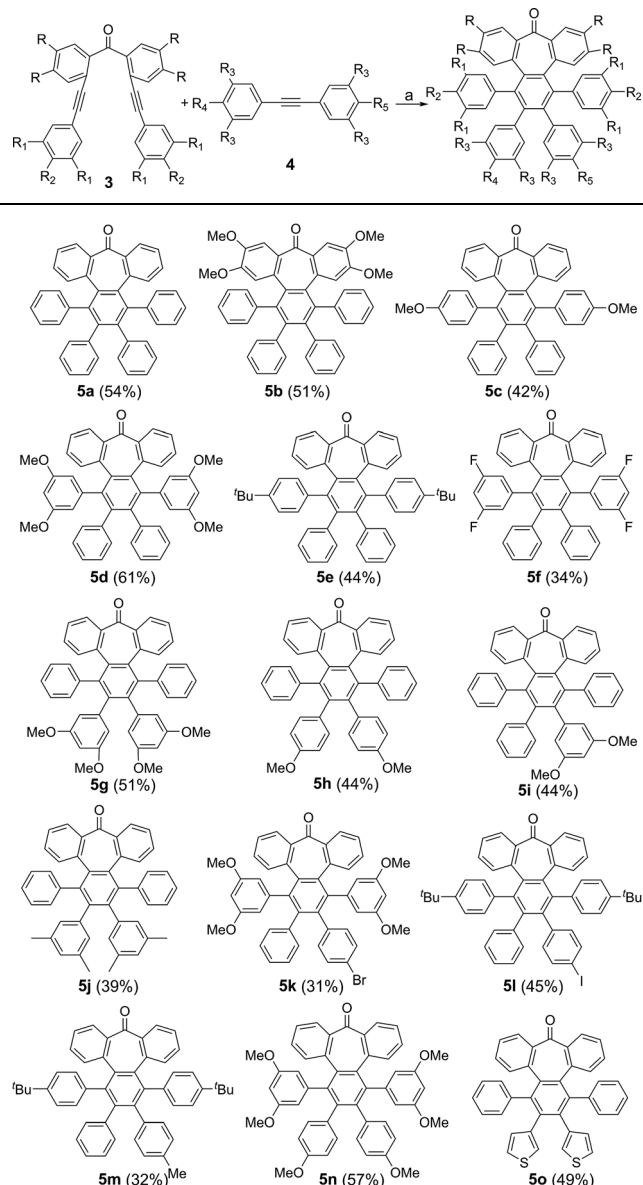
The scheme illustrates the synthetic route. It starts with a dialkyne **3** (represented as a central benzophenone-like core with two alkyne arms) reacting to form a heptagon-containing polycyclic arene **1** (a hexagonal ring with a heptagon in the center, and two 'Bu groups at the edges). This intermediate **1** then undergoes oxidative cyclodehydrogenation to form a distorted nanographene **2** (a hexagonal ring with a heptagon in the center, and two CHO groups at the edges).

- Simple and accessible starting materials
- Heptagon-containing polycyclic arene backbone in one single step
- Easy introduction of functional groups for further extension to larger structures

Scheme 1 General scheme, important features of synthetic approach, and structures of distorted expanded nanographenes prepared, **1** and **2**.



Table 1 General cyclotrimerization reaction and compounds prepared



^a Dialkyne 3 (0.1 mmol), diphenylacetylene 4 (0.15 mmol), Co₂(CO)₈ (0.13 mmol), 1,4-dioxane (6 mL), 100 °C, 16 h

being unchanged under similar conditions. In these cases, however, the combination DDQ/CF₃SO₃H was required and fully cyclodehydrogenated compounds 6e-g were isolated in good yields while forming five new C-C bonds. These distorted nanographenes can be considered as coronene analogues containing a seven-membered carbocycle in the otherwise hexagonal network. Similar nanographene 6h, incorporating methoxy groups, can be obtained by treatment of 6a with FeCl₃ in MeNO₂/DCE (60 °C, 16 h). In this case, the molecular packing of 6h in the X-ray crystal structure exhibits π-π interaction between molecules. The distance between two curved π-faces is

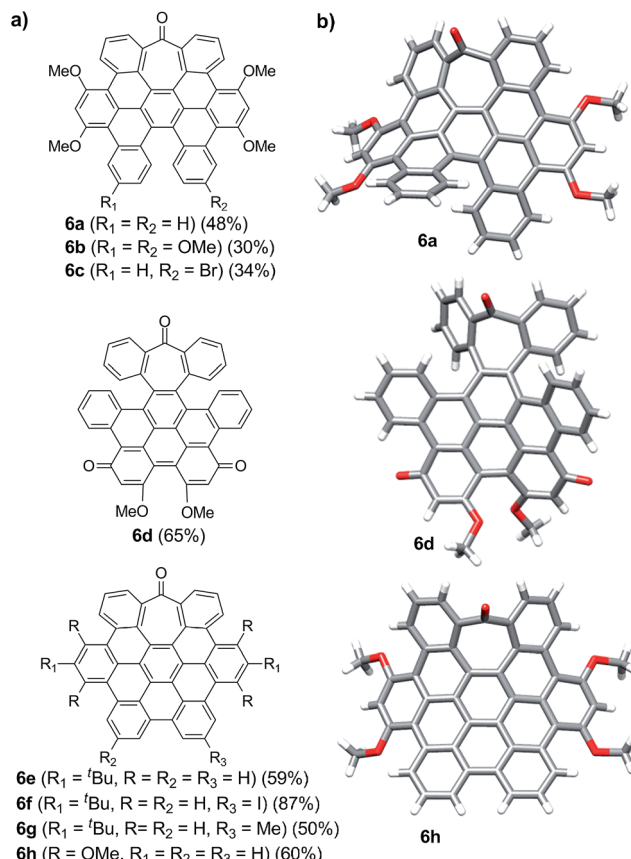


Fig. 1 (a) Heptagon-containing nanographenes. (b) Single crystal X-ray diffraction structures of 6a, 6d and 6h. Color code: C: gray, O: red, H: white.

3.8 Å, measured from the distance between two centroids of benzene rings.

The presence of π-interactions between molecules in these distorted nanographenes could support their application as organic semiconductors in the solid state. In this sense, we performed the calculation of the electronic and transport properties of the relaxed stacked 6h structure, following the stacking data obtained by X-ray measurements and relaxing the chain coordinates *via* total energy minimization until changes in the forces were below 0.02 eV Å⁻¹. In this manner, the calculated band structure possesses a gap of 1.71 eV (see ESI, Fig. S6† for the calculated conductance, density of states and band structures of the stacked 6h nanographenes). In order to elucidate the influence of the defect on the transport and electronic properties of the 6h nanographenes, a similar analysis was performed for a related planar coronene, resulting in a close gap value of 1.75 eV (see ESI, Fig. S7†). Taking into account its high solubility, crystallinity in the solid state, and the calculated gap value, we anticipate that 6h could be a promising candidate for the future development of printable organic field-effect transistors (OFETs).

While the inclusion of methoxy substituents is required for the cyclodehydrogenation event, we wondered whether these motifs could be utilized as coupling partners *via* C-OMe

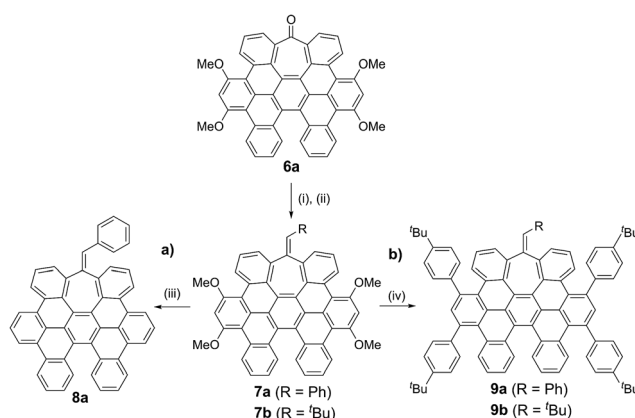


cleavage.¹⁵ Prompted by our recent work on Ni-catalyzed hydrogenolysis of aryl methyl ethers,¹⁶ we could easily obtain all-carbon heptagon-containing distorted nanographene **8a** in 80% yield upon exposure of **7a** under a $\text{Ni}(\text{cod})_2/\text{PCy}_3$ regime, using tetramethyldisiloxane (TMDSO) as the reducing agent (Scheme 2a).

This result is particularly noteworthy, as producing rather elusive all-carbon doubly distorted nanographenes is now within reach, representing a testament of the prospective impact of the Ni-catalyzed C-OMe bond-cleavage reactions.

More interestingly, **7a** and **7b** were found to be competent in Kumada-Tamao-Corriu reactions *via* C-OMe cleavage,¹⁷ rapidly furnishing **9a** and **9b** in good yields (Scheme 2b). The direction chosen to enlarge the aromatic backbone means that the seven-membered carbocycle would be allocated in the middle and at the edge of the all-carbon structure, suggesting that these compounds could result in strong electron hole conductance asymmetry.¹⁸ Subsequently, **9a** was submitted to oxidative dehydrogenation conditions with DDQ/MeSO₃H in CH_2Cl_2 , obtaining as the major product (47%) a highly distorted extended nanographene **1** that was firstly characterized by MALDI-TOF.¹⁹ As depicted in Fig. S82 (see ESI†) there is only one dominant peak in the mass spectrum of **1** and the isotopic distribution pattern of the high-resolution mass peak is in good agreement with the calculated patterns (Fig. S83, see ESI†). ¹H-NMR spectroscopy of compound **1** showed broad signals at room temperature. This fact is not related to the solubility of the compound. The rotation of the pendant aromatic rings (Fig. 2, red aromatic rings) is slow at room temperature, yielding poorly resolved signals. VT-NMR spectroscopy in 1,1,2,2-tetrachloroethane-*d*₂ at 369 K allowed us to unambiguously assign the distorted structure of **1** (Fig. 2b).

More interestingly, a simple exposure of **9b** under classical oxidative dehydrogenation conditions did not only result into two new aromatic rings, but also led to a new edge-sharing



Scheme 2 Subsequent transformations of heptagon-containing nanographene **6a**: (a) synthesis of all-carbon distorted nanographene **8a** containing both heptagon and [5]-helicene motifs. (b) Ni-Catalyzed KTC coupling in distorted nanographenes. Reaction conditions: (i) PhCH_2MgCl (**7a**) or $\text{tBuCH}_2\text{MgCl}$ (**7b**), THF, RT, 2 h. (ii) SOCl_2 , Py_{anh} , RT, 1 h, 54% (**7a**), 47% (**7b**) (2 steps). (iii) $\text{Ni}(\text{cod})_2$, PCy_3 , TMDSO, toluene, $100\text{ }^\circ\text{C}$, 16 h, 80%. (iv) $\text{Ni}(\text{cod})_2$, PCy_3 , *p*-*t*BuPhMgBr, toluene, $100\text{ }^\circ\text{C}$, 16 h, 79% (**9a**), 59% (**9b**).

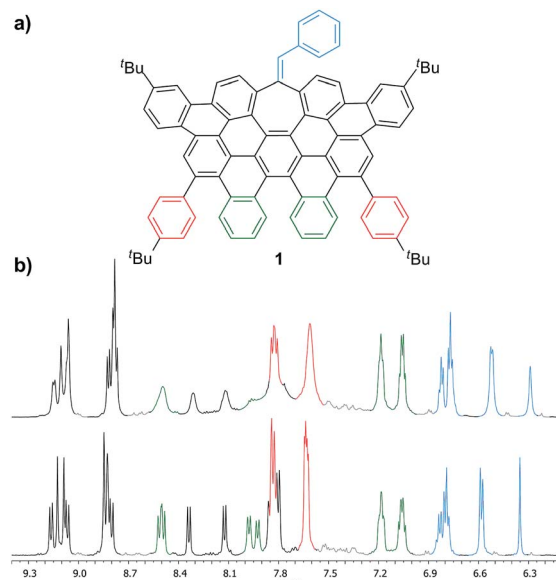


Fig. 2 (a) Structure of **1** and (b) partial ¹H-NMR spectra (500 MHz, $\text{C}_2\text{D}_2\text{Cl}_4$) of **1** at: 293 K (top) and 369 K (bottom).

heptagon–pentagon combination at the border of the expanded graphene molecule **2**. Compound **2**, obtained in 44% yield, was characterized by MALDI-TOF and VT-NMR in DMSO-d_6 at 348 K (see ESI, Fig. S84 and S87, respectively†). In this case, the structure of **2** was also confirmed by X-ray crystallography (Fig. 3), revealing that the π -backbone adopts a curved shape caused by the pentagon–heptagon unit and the chiral twisted conformation caused by the [5]-helicene moiety. The torsion angle in the helicene region resulted in 37° being the angle between the terminal helicene rings of 76° (Fig. 3, blue rings). We observed distorted benzene rings, with torsion angles up to 28° (Fig. 3, green ring) with the angle between the planes defined by carbon atoms 1–3 and 4–6 being 38° (see ESI, Fig. S1†). The huge distortion from planarity avoids strong π – π interactions between molecules and therefore enhances solubility in common organic solvents. The side *t*-butyl groups also improve solubility, where this molecule with 88 carbon atoms, a length of *ca.* 15.5 Å and width of *ca.* 9.7 Å, is highly soluble even in hexane.

The observed regioselectivity in the cyclodehydrogenation for **9a** and **9b** can be rationalized with the aid of theoretical

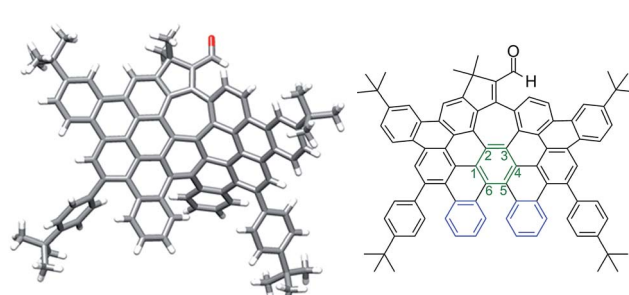


Fig. 3 Distorted graphene molecule **2**: single crystal structure (left) and corresponding ChemDraw structure (right).

calculations. We performed a detailed theoretical study on the activation barriers for different protonation/cyclization sites.

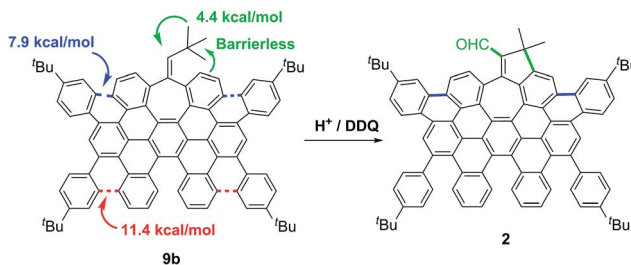
After initial structure optimization using DFT with B3LYP and the 6-31G(d,p) basis set, further optimization was carried out at the M06-2X/6-311+G(d,p) level of theory in a solvent model (IEFPCM) and the stationary points were characterized by frequency calculations in order to verify that they have the right number of imaginary frequencies. Thus, the energies and coordinates of the lowest energy transition state of each ring closure after each position was protonated were obtained (see ESI, Tables S4 and S5†).

Hence, in agreement with the experimental results, the theoretical data showed that the carbocationic species, formed upon protonation of the aromatic rings in **9a** and **9b**, suffer facile cyclization. Particularly cyclizations *en route* to **1** and **2** have lower activation energies ($\Delta E^\ddagger = 7.9$, $\Delta G^\ddagger = 10.1$ kcal mol⁻¹ for **9a** and $\Delta E^\ddagger = 7.9$, $\Delta G^\ddagger = 8.8$ kcal mol⁻¹ for **9b**, Scheme 3, blue). Theoretical calculations also suggest that the presence of the five membered ring in compound **2** derives from the protonation of the exocyclic double bond of **9b**, triggering a fast methyl group migration ($\Delta G^\ddagger = 4.4$ kcal mol⁻¹) and a subsequent barrierless electrophilic aromatic substitution (Scheme 3, green. See ESI, Fig. S9†).

Final DDQ-mediated dehydrogenation and oxidation of the allylic moiety give rise to the corresponding conjugated aldehyde.²⁰

Optical and electrochemical properties

We evaluated the optical and electrochemical properties of **1** and **2**. Shown in Fig. 4 are the absorption and fluorescence spectra of **1** and **2** in CH_2Cl_2 . UV-Vis spectra of both compounds showed a very strong absorption band centered at about 385 nm. Optical band gaps of **1** and **2** can be estimated from the longest absorption wavelength as 2.48 and 2.16 eV, respectively, which are in the range of known organic semiconductors.²¹ Notably, compounds **1** and **2** exhibited similar shaped fluorescence patterns when irradiated with UV light, including one intense blue fluorescence in CH_2Cl_2 centered at 495 nm followed by a shoulder peak at 530 nm. Their structured emission spectra are characterized by a vibronic progression indicative of a rigid aromatic fluorophore. Compound **2** also showed a broad emission band centered at 590 nm which can be assigned to the conjugated aldehyde chromophore. Both distorted extended nanographenes **1** and **2** showed similar quantum efficiencies



Scheme 3 Summary of calculated energies of subsequent transformations of **9b** upon protonation.

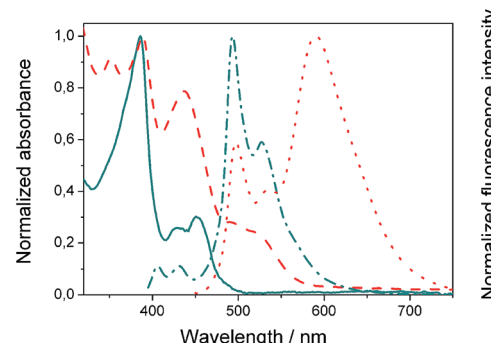


Fig. 4 Normalized absorbance of compound **1** (—) and **2** (---) in CH_2Cl_2 and corresponding normalized fluorescence emission spectra upon excitation at 385 (---) and 440 (···) nm, respectively.

(Φ) of 7.2 and 7.5%, respectively. Fluorescence lifetimes were also evaluated for both compounds as $\tau_1 = 14.5$ ns and $\tau_2 = 4.1$ ns for **1** and $\tau_1 = 12.9$ ns and $\tau_2 = 3.7$ ns for **2**. These exceptionally long fluorescence lifetimes of 14.5 and 12.9 ns are significantly longer than that of related fluorescent dyes, such as perylene bisimides.²² Time Resolved Emission Spectroscopy (TRES) allowed the complete deconvolution of the total emission spectrum by recovering the species-associated emission spectra (SAEMS) for each one of the decay times (Fig. 5).

We could confirm in both cases the presence of two main emissive species. In the case of **1**, both species were centered at 495 nm and maintained their original rigid aromatic fluorophore, owing to their characteristic vibronic progression. The presence of the two diastereomeric species, owing to the presence of both a helicene-like moiety and a non-planar unit, might be responsible for the observed emission spectra, given that the interconversion between diastereomers is slower than the emission process. The species with the shorter decay time ($\tau_2 = 4.1$ ns) dominated the emission. The longer one ($\tau_1 = 14.5$ ns) could derive from some minor structural changes, possibly due to the presence of the pendant phenyl group in **1** (Fig. 2, blue). For **2**, only the component with the longer lifetime ($\tau_2 = 12.9$ ns) kept the rigid fluorophore emitting at 495 nm, while the species with the shorter decay time ($\tau_1 = 3.7$ ns) is responsible for the broad emission centered at 590 nm.

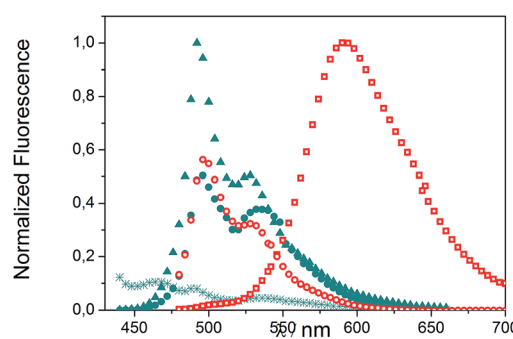


Fig. 5 TRES deconvolution of compounds **1**: $\tau_1 = 14.5$ ns (●), $\tau_2 = 4.1$ ns (▲) and **2**: $\tau_1 = 3.7$ ns (□), $\tau_2 = 12.9$ ns (○) in CH_2Cl_2 .



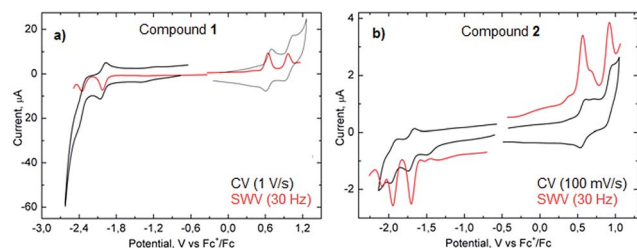


Fig. 6 CV and SWV of compound 1 (a) and 2 (b) in CH_2Cl_2 .

Measurements of the electrochemical behavior of compounds **1** and **2** were possible because they both have sufficient solubility in common organic solvents such as chloroform, dichloromethane and even hexane. In CH_2Cl_2 , both **1** and **2** display two reversible oxidation waves with first and second oxidation potentials of +0.64 and +0.96 V and +0.58 and +0.91 V (vs. Fc^+/Fc), respectively (Fig. 6). In the negative potential region, two reversible reduction waves were observed with first and second reduction potentials of -2.02 and -2.36 V (vs. Fc^+/Fc) for **1** and -1.69 and -1.95 V (vs. Fc^+/Fc) for **2**. Hence, the HOMO-LUMO energy gaps for **1** and **2** based on the first half-wave oxidation and reduction potentials resulted in 2.66 eV and 2.27 eV, respectively, which are in the range of previously described extended aromatic systems.²³ Therefore, enlarged distorted nanographenes may become attractive candidates for diverse applications such as organic field effect transistors and solar cells.

Conclusions

We have demonstrated that a wide variety of distorted heptagon-containing nanographene precursors can be easily prepared from simple building blocks by a Co-catalyzed cyclo-trimerization reaction. The versatility of this method allows easy introduction of functional groups, affording a selection of distorted nanographenes. Furthermore, these nanostructures can be easily enlarged by the combination of Ni-catalyzed cross-coupling and cyclodehydrogenation reactions. Following this approach we have successfully presented highly distorted derivatives **1** and **2**. Notably, distorted PAHs **1** and **2** exhibited interesting optical and electronic properties, with exceptionally long fluorescence lifetimes (14.5 and 12.9 ns, respectively) and promising low band gaps (2.66 and 2.27 eV, respectively). Remarkably, both compounds resemble the elementary structural topological defects in graphene disclinations as heptagons and dislocations as a pair of edge-sharing pentagon-heptagons. The ability to chemically tailor heptagon-containing nanographenes and GNRs in a well-defined manner would help to clarify the properties of defective graphene, and pave the way for the development of distorted graphene molecule-based devices for nanoelectronics and optoelectronics.

Acknowledgements

This project has received funding from the European Research Council (ERC) under the European Union's Horizon 2020

research and innovation program (ERC-2015-STG-677023 - NANOGRAPHOUT). We thank the Ministerio de Economía y Competitividad (MINECO, Spain) (CTQ2014-53598-R, TEC2014-59730). A. G. C. and B. B. gratefully acknowledge funding from MINECO for RyC-2013-12943 and RYC-2012-10381 contracts. I. R. M. thanks MECD (Spain) for a predoctoral FPU fellowship. D. C. L. thanks Intramural CSIC project (201530E01). We also thank IZO-SGI SGIker of UPV/EHU for their technical and human support and computational resources provided by the RES and the CSIRC-Alhambra supercomputing facilities.

Notes and references

- Reviews on the synthesis of planar PAHs: (a) M. D. Watson, A. Fechtenkötter and K. Müllen, *Chem. Rev.*, 2001, **101**, 1267–1300; (b) J. Wu, W. Pisula and K. Müllen, *Chem. Rev.*, 2007, **107**, 718–747; (c) M. G. Schwab, A. Narita, Y. Hernandez, T. Balandina, S. D. Feyter, X. Feng and K. Müllen, *J. Am. Chem. Soc.*, 2012, **134**, 18169–18172; (d) A. Narita, X. Feng, Y. Hernandez, S. A. Jensen, M. Bonn, H. Yang, I. A. Verzhbitskiy, C. Casiraghi, M. R. Hansen, A. H. R. Koch, G. Fytas, O. Ivasenko, B. Li, K. S. Mali, T. Balandina, S. Mahesh, S. De Feyter and K. Müllen, *Nat. Chem.*, 2014, **6**, 126–132; (e) J. Liu, B.-W. Li, Y. Tan, A. Giannakopoulos, C. Sanchez-Sanchez, D. Beljonne, P. Ruffieux, R. Fasel, X. Feng and K. Müllen, *J. Am. Chem. Soc.*, 2015, **137**, 6097–6103; (f) U. Beser, M. Kastler, A. Maghsoumi, M. Wagner, C. Castiglioni, M. Tommasini, A. Narita, X. Feng and K. Müllen, *J. Am. Chem. Soc.*, 2016, **138**, 4322–4325.
- (a) A. Hashimoto, K. Suenaga, A. Gloter, K. Urita and S. Iijima, *Nature*, 2004, **430**, 870–873; (b) P. Y. Huang, C. S. Ruiz-Vargas, A. M. van der Zande, W. S. Whitney, M. P. Levendorf, J. W. Kevek, S. Garg, J. S. Alden, C. J. Hustedt, Y. Zhu, J. Park, P. L. McEuen and D. A. Muller, *Nature*, 2011, **469**, 389–392.
- S. T. Skowron, I. V. Lebedeva, A. M. Popov and E. Bichoutskaia, *Chem. Soc. Rev.*, 2015, **44**, 3143–3176.
- O. V. Yazyev and Y. P. Chen, *Nat. Nanotechnol.*, 2014, **9**, 755–767.
- (a) V. M. Tsefrikas and L. T. Scott, *Chem. Rev.*, 2006, **106**, 4868–4884; (b) Y. T. Wu and J. S. Siegel, *Chem. Rev.*, 2006, **106**, 4843–4867.
- K. Yamamoto, T. Harada and M. Nakazaki, *J. Am. Chem. Soc.*, 1983, **105**, 7171–7172.
- (a) J. Luo, X. Xu, R. Mao and Q. Miao, *J. Am. Chem. Soc.*, 2012, **134**, 13796–13803; (b) K. Y. Cheung, X. Xu and Q. Miao, *J. Am. Chem. Soc.*, 2015, **137**, 3910–3914; (c) Q. Miao, *Chem. Rev.*, 2015, **15**, 1156–1159.
- (a) A. Pradhan, P. Dechambenoit, H. Bock and F. Durola, *J. Org. Chem.*, 2013, **78**, 2266–2274; (b) E. U. Mughal and D. Kuck, *Chem. Commun.*, 2012, **48**, 8880–8882.
- (a) K. Kawasumi, Q. Zhang, Y. Segawa, L. T. Scott and K. Itami, *Nat. Chem.*, 2013, **5**, 739–744; (b) K. Kato, Y. Segawa, L. T. Scott and K. Itami, *Chem.-Asian J.*, 2015, **10**, 1635–1639.



10 (a) A. Narita, X. Feng and K. Müllen, *Chem. Rec.*, 2015, **15**, 295–309; (b) A. Narita, X.-Y. Wang, X. Feng and K. Müllen, *Chem. Soc. Rev.*, 2015, **44**, 6616–6643.

11 W. Baidossi, H. Schumann and J. Blum, *Tetrahedron*, 1996, **52**, 8349–8364.

12 (a) B. T. King, J. Kroulík, C. R. Robertson, P. Rempala, C. L. Hilton, J. D. Korinek and L. M. Gortari, *J. Org. Chem.*, 2007, **72**, 2279–2288; (b) L. Zhai, R. Shukla and R. Rathore, *Org. Lett.*, 2009, **11**, 3474–3477; (c) Cyclodehydrogenation promoted by FeCl_3 was avoided to prevent formation of chlorinated products.

13 J. L. Ormsby, T. D. Black, C. L. Hilton, Bharat and B. T. King, *Tetrahedron*, 2008, **64**, 11370–11378.

14 (a) S. Xiao, S.-J. Kang, Y. Wu, S. Ahn, J. B. Kim, Y.-L. Loo, T. Siegrist, M. L. Steigerwald, H. Li and C. Nuckolls, *Chem. Sci.*, 2013, **4**, 2018–2023; (b) A. L. Pinardi, J. I. Martínez, A. Jančářík, I. G. Stará, I. Starý, M. F. López, J. Méndez and J. Á. Martín-Gago, *Chem. Commun.*, 2014, **50**, 1555–1557; (c) T. Fujikawa, Y. Segawa and K. Itami, *J. Am. Chem. Soc.*, 2015, **137**, 7763–7768; (d) X. Gu, X. Xu, H. Li, Z. Liu and Q. Miao, *J. Am. Chem. Soc.*, 2015, **137**, 16203–16208; (e) L. Shan, D. Liu, H. Li, X. Xu, B. Shan, J. B. Xu and Q. Miao, *Adv. Mater.*, 2015, **27**, 3418–3423; (f) T. Fujikawa, Y. Segawa and K. Itami, *J. Am. Chem. Soc.*, 2016, **138**, 3587–3595; (g) D. Peña, D. Pérez, E. Gutián and L. Castedo, *Org. Lett.*, 1999, **1**, 1555–1557; (h) X. Feng, J. Wu, V. Enkelmann and K. Müllen, *Org. Lett.*, 2006, **8**, 1145–1148.

15 Reviews on metal-catalyzed reactions involving the cleavage of C–O bonds: (a) J. Cornella, C. Zarate and R. Martin, *Chem. Soc. Rev.*, 2014, **43**, 8081–8097; (b) B. Su, Z. C. Cao and Z. J. Shi, *Acc. Chem. Res.*, 2015, **48**, 886–896; (c) M. Tobisu and N. Chatani, *Acc. Chem. Res.*, 2015, **48**, 1717–1726.

16 P. Álvarez-Bercedo and R. Martin, *J. Am. Chem. Soc.*, 2010, **132**, 17352–17353.

17 For Ni-catalyzed cross-coupling of methoxyarenes and ArMgX see: (a) E. Wenkert, E. L. Michelotti and C. S. Swindell, *J. Am. Chem. Soc.*, 1979, **101**, 2246–2247; (b) E. Wenkert, E. L. Michelotti, C. S. Swindell and M. Tingoli, *J. Org. Chem.*, 1984, **49**, 4894–4899; (c) J. W. Dankwardt, *Angew. Chem.*, 2004, **43**, 2428–2432; (d) B.-T. Guan, S.-K. Xiang, T. Wu, Z.-P. Sun, B.-Q. Wang, K.-Q. Zhao and Z.-J. Shi, *Chem. Commun.*, 2008, **2**, 1437–1439; (e) J. Cornella and M. Ruben, *Org. Lett.*, 2013, **15**, 6298–6301; (f) M. Tobisu, T. Takahira and N. Chatani, *Org. Lett.*, 2015, **17**, 4352–4355.

18 S. M. M. Dubois, A. Lopez-Bezanilla, A. Cresti, F. Triozon, B. Biel, J. C. Charlier and S. Roche, *ACS Nano*, 2010, **4**, 1971–1976.

19 Typical reaction conditions: DDQ (3 equiv.) in $\text{CH}_2\text{Cl}_2/\text{MeSO}_3\text{H}$ (40/1), 10 min, RT. Longer reaction times and a higher amount of DDQ led to a mixture of different products derived from subsequent cyclodehydrogenation reactions, which could not be properly isolated and characterized.

20 The oxidation requires the presence of water that comes from the MeSO_3H used. Similar allylic oxidation with DDQ has been previously reported: H. Lee and R. G. Harvey, *J. Org. Chem.*, 1983, **48**, 749–751.

21 J. C. S. Costa, R. J. S. Taveira, C. F. R. A. C. Lima, A. Mendes and L. M. N. B. F. Santos, *Opt. Mater.*, 2016, **58**, 51–60.

22 F. Würthner, *Chem. Commun.*, 2004, 1564–1579.

23 (a) Z. Sun, Q. Ye, C. Chi and J. Wu, *Chem. Soc. Rev.*, 2012, **41**, 7857–7889; (b) T. Dumslaff, B. Yang, A. Maghsoumi, G. Velpula, K. S. Mali, C. Castiglioni, S. De Feyter, M. Tommasini, A. Narita, X. Feng and K. Müllen, *J. Am. Chem. Soc.*, 2016, **138**, 4726–4729.

